Available online at www.sciencedirect.com
ScienceDirect
Acta Materialia 58 (2010) 4883–4890
Acta MATERIALIA
www.elsevier.com/locate/actamat

Criteria for tensile plasticity in Cu–Zr–Al bulk metallic glasses

S. Pauly [a,*], G. Liu [b], S. Gorantla [a], G. Wang [a], U. Kühn [a], D.H. Kim [c], J. Eckert [a,d]

[a] IFW Dresden, Institut für Komplexe Materialien, Helmholtzstraße 20, D-01069 Dresden, Germany
[b] State Key Laboratory for Mechanical Behavior of Materials, School of Materials Science and Engineering, Xi'an Jiaotong University, Xi'an 710049, China
[c] Center for Non-Crystalline Materials, Department of Metallurgical Engineering, Yonsei University, Seoul 120-749, Republic of Korea
[d] TU Dresden, Institut für Werkstoffwissenschaft, D-01062 Dresden, Germany

Received 4 February 2010; received in revised form 24 March 2010; accepted 11 May 2010
Available online 9 June 2010

Abstract

$(Cu_{0.5}Zr_{0.5})_{100-x}Al_x$ ($x = 5$, 6, 8) bulk metallic glasses (BMGs) were deformed in tension. Besides ductility up to 0.5%, the material shows work-hardening behaviour. Both effects are attributed to the deformation-induced precipitation of B2 CuZr nanocrystals and the formation of twins in the nanocrystals larger than 20 nm. The precipitation of the nanocrystals alters the stress field in the matrix and is expected to retard shear band propagation, which in turn allows stresses in the nanocrystals to rise. This stress build-up is more severe in the larger grains and might be responsible for the subsequent twinning. Both deformation-induced nanocrystallization and twinning consume energy and avoid crack formation and with it premature failure.
© 2010 Acta Materialia Inc. Published by Elsevier Ltd. All rights reserved.

Keywords: Bulk metallic glasses; Tensile tests; Ductility; Twinning; Martensitic transformation

1. Introduction

Bulk metallic glasses (BMGs) generally suffer from brittle and thus catastrophic failure as they deform inhomogeneously at room temperature under quasi-static loading conditions [1–3]. Plastic strain is localized in regions of only a few tens of nanometres thickness, the so-called shear bands [4–7]. Even though the strain can be as high as 10 within the shear bands [8], their volume fraction is usually limited and thus their overall contribution to the macroscopic plastic deformation is negligible [1,9]. There are different approaches to enhancing the plasticity of BMGs [10]. One way is to introduce a second phase into the material [11]. Among the in situ BMG matrix composites, CuZr-based alloys have been shown to be promising candidates [12–15]. This can be traced back to the fact that the crystalline phase, which forms in these composites, B2 CuZr, is rather ductile and furthermore is a shape memory alloy [13,16,17]. Therefore, it exhibits a reversible martensitic transformation, which is responsible for the significant work-hardening of this phase [13,16–18]. These two peculiarities, i.e. that binary CuZr is a bulk glass-former and at the same time is a shape memory alloy in its crystalline state, constitute the interesting phenomena observed in these alloys.

As a matter of fact these particular aspects are also crucial for the deformation behaviour described in this paper. Here, we report on the intrinsic toughening mechanism of CuZr-based BMGs deformed under tensile loading conditions, which results in macroscopically detectable plasticity.

2. Experimental

The pre-alloys were prepared by arc-melting proper amounts of the pure elements. To ensure efficient mixing the ingots were re-melted at least three times prior to casting. The pre-alloys were consecutively cast in a water-cooled Cu mould attached to the arc-melter. The resulting plates had dimensions of $0.15 \times 1 \times 6\ cm^3$ and were cut into dog bone geometry using spark-wire erosion. The ten-

* Corresponding author.
E-mail address: s.pauly@ifw-dresden.de (S. Pauly).

1359-6454/$36.00 © 2010 Acta Materialia Inc. Published by Elsevier Ltd. All rights reserved.
doi:10.1016/j.actamat.2010.05.026

sile tests were performed in an Instron 5869 with an initial strain rate of $1 \times 10^{-4}\,s^{-1}$. The strain was measured directly at the sample by means of a Fiedler laser extensometer. The elastic regime was fitted linearly and the point where the strain deviated from linearity was chosen as onset of plasticity. At least four specimens of each composition were tested to ensure reproducibility of the results. Additionally, the elastic constants were determined by ultrasound velocity measurements (Olympus Panametrics-NDT 5900PR). Transmission electron microscopy (TEM) was done with a Tecnai F30 equipped with a field emission gun (FEG) and operated at an accelerating voltage of 300 kV. The samples for the TEM investigation were thinned manually and then made electron-transparent by ion-milling using a Gatan 691 Precision Ion Polishing System with a liquid nitrogen cooling system. The energy of the ion beam was 2.5 keV and the ion-milling time duration was 2.5–3 h. The thermal stability of the three alloys was determined at a heating rate of 40 K min^{-1} in a Perkin–Elmer Diamond differential scanning calorimeter (DSC).

3. Results and discussion

3.1. Deformation-induced microstructural changes and plasticity

Fig. 1 shows the true stress–strain curves obtained under tensile loading. There is a clear deviation from linearity and

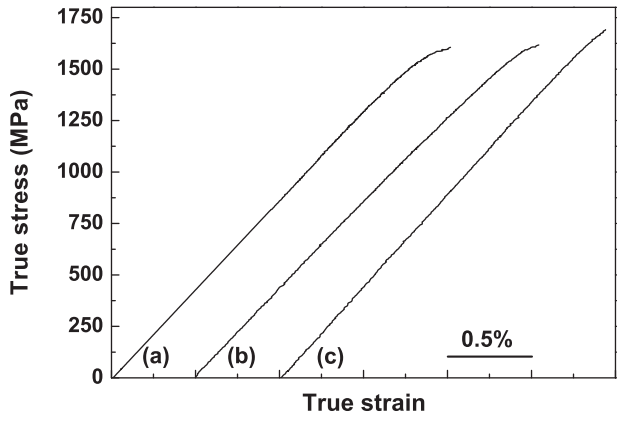

Fig. 1. True stress–strain curves in tensile loading for (a) $Cu_{47.5}Zr_{47.5}Al_5$, (b) $Cu_{47}Zr_{47}Al_6$ and (c) $Cu_{46}Zr_{46}Al_8$. All alloys show a certain degree of yielding. A plasticity of up to 0.5% can be detected. The inset depicts the surface of a $Cu_{47.5}Zr_{47.5}Al_5$ BMG after fracture and, clearly, shear offsets due to shear banding are mostly absent.

furthermore the detectable ductility is accompanied by work-hardening. The Young's modulus is identical for all three alloys within the experimental error (about 87 ± 5 GPa, Table 1), which compares well with results of ultrasound velocity measurements and with results reported for compression tests [13]. Yet, the fracture strength increases with increasing Al content, the same trend that the glass transition temperature, T_g, follows (Table 1). Both the strength of bulk metallic glasses as well as their glass transition temperature have been attributed to the atomic bond strength [19,20]. Indeed, the ratio of fracture strength-to-glass transition temperature, σ_f/T_g, remains nearly constant (Table 1), which means that the addition of Al increases the strength as well as the glass transition temperature roughly by the same factor. Therefore, the addition of Al is assumed to enhance the bond strength, which reflects in a higher glass transition temperature and an increased ultimate tensile strength. Another effect of the enhanced bond strength is the increased critical casting thickness with an increasing amount of Al [21–23].

The plastic strain is largest for $Cu_{47.5}Zr_{47.5}Al_5$ with $0.50 \pm 0.05\%$ and gradually decreases to a value of $0.05 \pm 0.02\%$ in the case of $Cu_{46}Zr_{46}Al_8$ (Table 1). Fig. 2 shows the surface of a $Cu_{47.5}Zr_{47.5}Al_5$ specimen after fracture and it is obvious that shear steps on the surface of the specimens due to shear banding are almost absent. This finding is rather striking, as plastic deformation of BMGs is generally borne by shear bands [1,9,24]. As a consequence a high density of shear bands is indicative of a large plastic deformability and the lack of shear bands in turn usually results in brittle behaviour [1,3]. However, in the present case the observed plasticity cannot be explained by extensive formation of shear bands (Fig. 2).

In order to reveal the mechanisms behind this rather unique deformation behaviour, TEM investigations were carried out. In the as-cast state, all alloys are glassy. Fig. 3 exemplarily displays the microstructure of a $Cu_{47.5}Zr_{47.5}Al_5$ specimen. The high-resolution image and the corresponding diffraction image do not give any hints for the presence of a crystalline phase. Yet, in some regions of the specimen sparse nanocrystals with typical diameters of 2–5 nm were observed (not shown here). After fracture the microstructure has clearly changed and abundant nanocrystals are embedded in the glassy matrix (Fig. 4). The density of nanocrystals has increased significantly and at the same time the nanocrystals have grown to diameters of up to 10–50 nm. Most importantly, the nanocrys-

Table 1
Elastic and plastic properties of the different $(Cu_{0.5}Zr_{0.5})_{100-x}Al_x$ alloys. E denotes the Young's modulus as obtained from the compression tests, E_{UT} the Young's modulus obtained from ultrasound velocity measurements, ε_p the plastic strain, ε_f the fracture strain, σ_f the fracture strength, f_{CuZr} crystalline volume fraction, $\overline{D}_{CuZr}$ the average B2 CuZr crystal size, L_{CuZr} the average inter-particle spacing, and T_g the glass transition temperature.

Composition	E (GPa)	E_{UT} (GPa)	ε_p (%)	ε_f (%)	σ_f (MPa)	f_{CuZr} (vol.%)	$\overline{D}_{CuZr}$ (nm)	L_{CuZr} (nm)	T_g (K)	σ_f/T_g (MPa/K)
$Cu_{47.5}Zr_{47.5}Al_5$	87 ± 5	88 ± 2	0.50 ± 0.05	2.02 ± 0.1	1600 ± 10	17.6 ± 1.1	20 ± 5	30 ± 10	702 ± 2	2.28
$Cu_{47}Zr_{47}Al_6$	84 ± 5	90 ± 2	0.45 ± 0.05	2.04 ± 0.1	1620 ± 10	15.4 ± 1.5	20 ± 5	32 ± 8	708 ± 2	2.29
$Cu_{46}Zr_{46}Al_8$	89 ± 5	93 ± 2	0.05 ± 0.02	1.94 ± 0.1	1690 ± 10	6.4 ± 1.0	18 ± 5	59 ± 12	720 ± 2	2.34

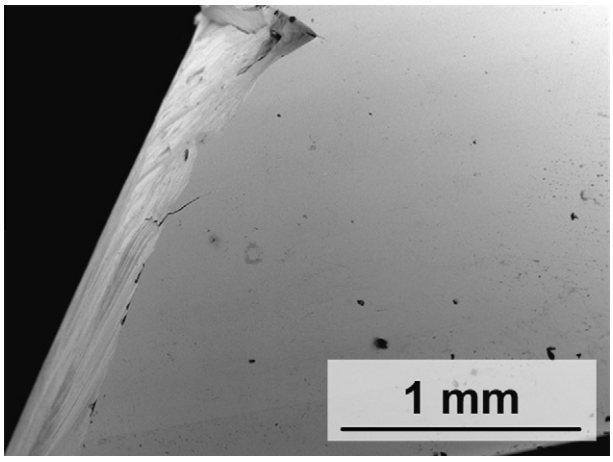

Fig. 2. Fractured $Cu_{47.5}Zr_{47.5}Al_5$ BMG, which clearly demonstrates that shear offsets due to shear banding are mostly absent.

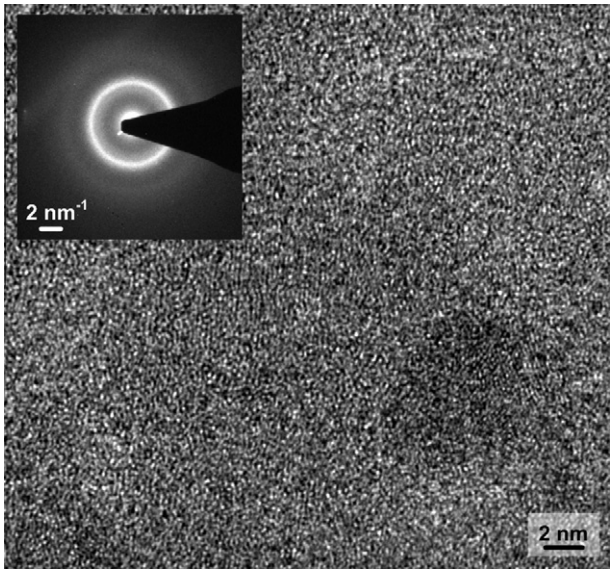

Fig. 3. TEM micrograph of $Cu_{47.5}Zr_{47.5}Al_5$ in the as-cast state. The inset shows the according electron diffraction pattern. Both images imply that the sample is monolithic glassy. In some regions, however, sparse nanocrystals with diameters of 2–5 nm can be found.

tallization appears to be a bulk phenomenon and not just restricted to shear bands, as has been observed for other BMGs [25–28]. Therefore, this energy-consuming phase transformation occurs in a sufficiently large volume to contribute to macroscopic ductility. Additionally, some of the larger nanocrystals show a contrast, which can be attributed to twinning, and which becomes especially apparent at higher magnification (inset in Fig. 4). The shape of the twinned nanocrystals tends to be more elliptical and in spite of this shape changes no cracking at the interfaces between particles and glassy matrix can be observed.

Electron diffraction reveals that these nanocrystals are B2 CuZr nanocrystals (Pm-3m) (Fig. 5), a phase which is stable only at temperatures above 988 K [29]. Most likely the precipitation of the B2 phase is kinetically favoured as it crystallizes polymorphically whereas the formation

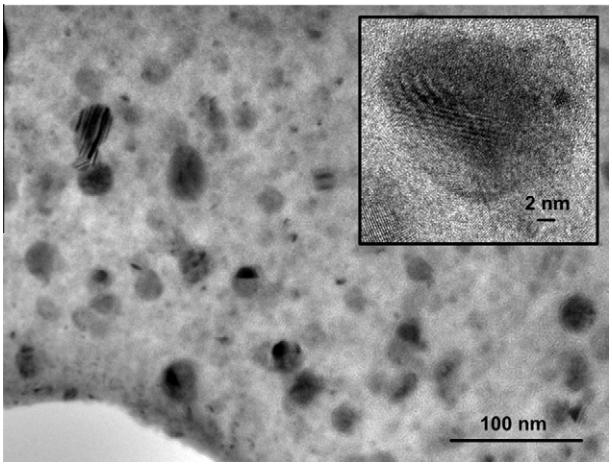

Fig. 4. A $Cu_{47.5}Zr_{47.5}Al_5$ specimen after deformation to fracture. The density of nanocrystals has increased and in the nanocrystals larger than 20 ± 5 nm twinning can be observed. The inset exhibits a twin at a higher magnification.

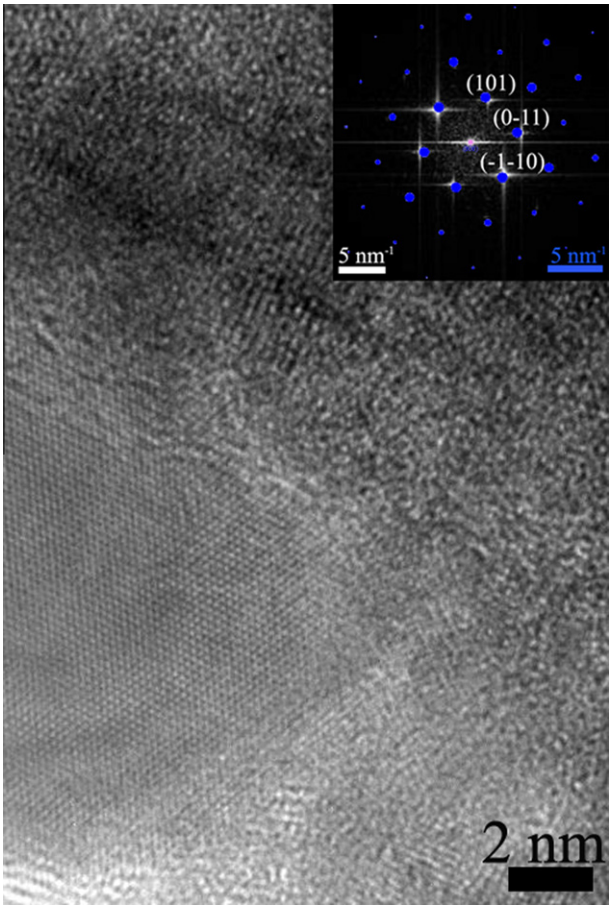

Fig. 5. HRTEM image of a B2 CuZr nanocrystal embedded in the glassy matrix. The diffraction pattern of the crystal can be indexed according to the B2 CuZr phase. The blue diffraction spots in the inset represent a simulated B2 structure (Pm-3m) using a lattice constant of $a_0 = 0.326$ nm and apparently there is a satisfying match between the observed and calculated diffraction pattern. (For interpretation of the references to colour in this figure legend, the reader is referred to the web version of this article.)

of the crystalline equilibrium phases $Cu_{10}Zr_7$ and $CuZr_2$ would require long-range diffusion. The deformation-induced crystallization and consecutive twinning found in the present alloys can be understood in the framework of the potential energy landscape (PEL) concept assuming a critical softening of the instantaneous shear modulus [30]. The interface between the crystal and the glassy matrix seems to be rather strong and no debonding or cracking can be observed (Fig. 5), which, when it occurs, reduces the ductility of such composites [31].

In order to exhibit these unique deformation processes the bulk metallic glass must possess the capability to precipitate polymorphically a shape memory alloy, which can undergo a deformation-induced martensitic transformation, such as B2 CuZr.

To gain a deeper understanding of the material's response to mechanical loading, the effect of the nanocrystalline precipitates and twinning on the evolution and propagation of shear bands is investigated in the next paragraphs. Our quantitative analysis will focus on the importance of growth of the nanocrystals along with the evolution of the proper inter-particle spacing on the one hand, and on factors influencing twinning, such as the grain size, on the other hand.

3.2. Growth of B2 CuZr nanocrystals and critical inter-particle spacing

At the early stages of deformation the B2 CuZr nanocrystals precipitate and continue to grow in the course of mechanical loading [30]. To get a more quantitative picture of the processes taking place during deformation, TEM images of the fractured specimen were evaluated and the crystallized volume fractions were determined. Since the particles are not ideal spheres but are rather elliptical in shape, an effective particle diameter was defined as [32,33]:

$$D_{\mathrm{CuZr}} = \sqrt{D_1 D_2} \tag{1}$$

where D_1 and D_2 are the smallest and largest diameter of a B2 CuZr nanocrystal. The volume fraction, f_{CuZr}, was then obtained assuming a thin foil projection and applying the following equation [34]:

$$f_{\mathrm{CuZr}} = \left(\frac{-2\pi\overline{D}_{\mathrm{CuZr}}}{\pi\overline{D}_{\mathrm{CuZr}} + 8t}\right)\ln(1-A) \tag{2}$$

where $\overline{D}_{\mathrm{CuZr}}$ is the mean particle size averaged over n particles ($\overline{D}_{\mathrm{CuZr}} = \left(\sum_{i=1}^{n} D_{\mathrm{CuZr}}\right)/n$, where n is the number of measured precipitates), t is the thickness of the foil and A is the projected area fraction of precipitates, which was obtained by the point count method [35] while truncation and overlapping of particles was accounted for [36]. In order to have a sound statistical foundation, at least 100 precipitates were measured. The particle size distributions of the alloys after fracture follow a Gauss distribution (not shown here) with a maximum at 20 ± 5 nm for $Cu_{47.5}Zr_{47.5}Al_5$ and $Cu_{47}Zr_{47}Al_6$ and with a maximum at 18 ± 5 nm for $Cu_{46}Zr_{46}Al_8$. Thus, the average particle size, $\overline{D}_{\mathrm{CuZr}}$, is roughly equal for all three alloys, which implies that the different plasticity of the alloys cannot be a result of the final crystal size. Conversely, the crystalline volume fraction strongly depends on the composition: it decreases from about 18 vol.% in $Cu_{47.5}Zr_{47.5}Al_5$ to about 6 vol.% in $Cu_{46}Zr_{46}Al_8$ (Table 1). This behaviour correlates well with the increasing glass-forming ability (GFA) and the stability of the supercooled liquid when Al is added to binary $Cu_{50}Zr_{50}$ [22,37]. It appears that a higher GFA results in a more sluggish precipitation of B2 nanocrystals during deformation of the bulk metallic glass and a lower ductility. There is a substantial growth of freshly nucleated B2 CuZr nanocrystals during deformation and the growth of the nanocrystals is all the more pronounced the lower the Al content, i.e. the less stable the glass (Table 1). Deformation-induced growth of body-centred cubic (bcc) nanocrystals embedded in a monatomic glassy matrix has been also observed in computer simulations [31], and the plastic strain such a composite exhibits upon compression has been attributed to this dynamic microstructural change [31]. It thus appears that the present results corroborate these simulations.

Moreover, further computer simulations have revealed that especially large nanocrystals (about twice as large as the shear band thickness) can effectively interact with nascent shear bands [38]. The grain sizes observed after fracture are on the right order of magnitude to ensure an interaction between the crystals and the local deformation concentrated in shear bands (Fig. 4 and Table 1).

Crystalline inclusions are known to alter the stress field in the matrix [38] and the interaction between the localized deformation in the matrix and the crystalline inclusions have a strong retarding effect on fracture [31]. As we will show below, in this process not only the grain size is of importance but also the average spacing between two adjacent particles.

Once the crystalline volume fraction and the average particle size are known one can calculate the average spacing between the particles, L_{CuZr}:

$$L_{\mathrm{CuZr}} = D_{\mathrm{CuZr}}\sqrt[3]{\frac{\pi}{6f_{\mathrm{CuZr}}}} \tag{3}$$

where D_{CuZr} is the particle size and f_{CuZr} is the crystalline volume fraction. The calculated inter-particle spacings should yield the same result as those determined experimentally and as is shown in Fig. 6a there is a satisfactory match between them. Consequently, the method used to calculate the geometrical relationship between the crystalline volume fractions and the inter-particle spacings is applicable in the present case.

In Fig. 6b, the measured crystalline volume fraction as well as the measured inter-particle spacing are plotted as function of composition. Naturally, the inter-particle spacing increases as the deformation-induced volume fraction of B2 CuZr decreases, provided the average particle diam-

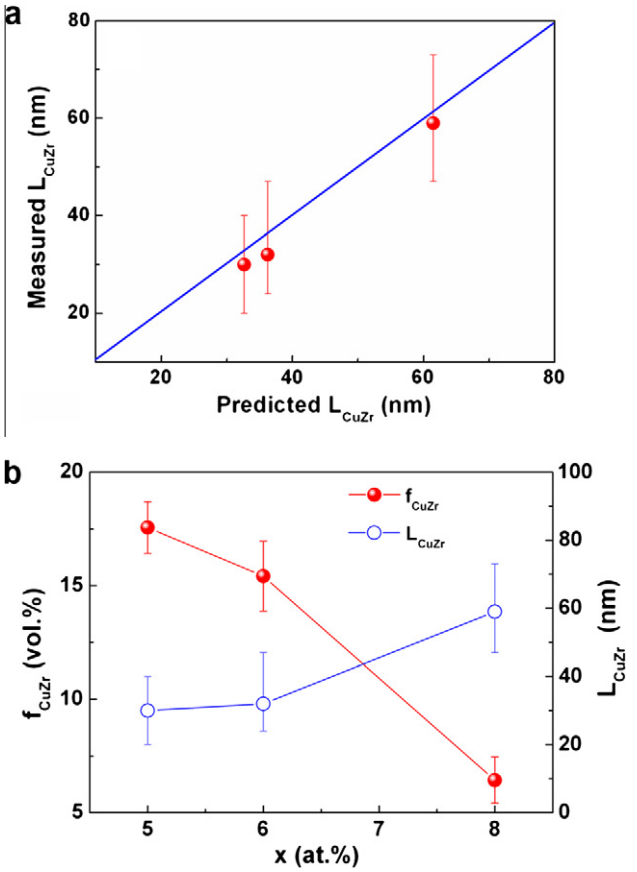

Fig. 6. (a) Measured and predicted inter-particle spacing. There is a good correspondence, which indicates that the applied model is capable of capturing the behaviour of the CuZr-based alloys. (b) Crystalline volume fraction, f_{CuZr}, and the inter-particle spacing, L_{CuZr}, as a function of the Al content.

eter remains constant, which is observed when the Al content is increased (Table 1).

Fig. 7 clearly shows the correlation between the inverse particle spacing, L_{CuZr}, and the plastic strain, ε_p. The inter-particle spacing of $Cu_{46}Zr_{46}Al_8$ (59 ± 12 nm) appears to be just around an extrapolated critical particle spacing of

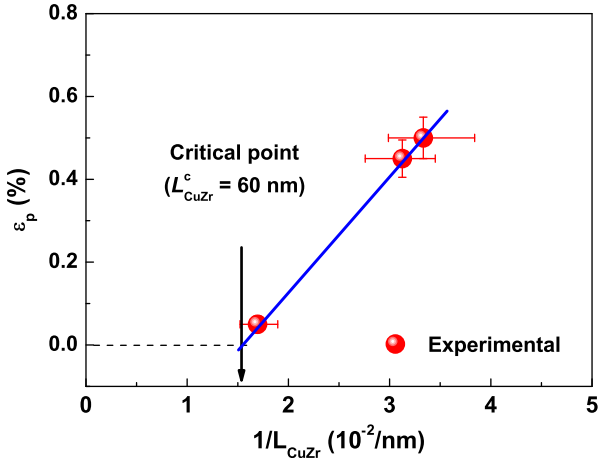

Fig. 7. Dependence of plastic strain on the crystalline volume fraction or equivalently on the inverse inter-particle spacing, $1/L_{CuZr}$.

$L^c_{CuZr} = 60 \pm 10$ nm, above which no ductility is to be expected. Even though the critical inter-particle spacing is slightly larger than the typical shear band thickness (20–50 nm) [5,7] the length-scales match quite well, especially, if one considers that such a heterogeneous microstructure is expected to result in a wavy shear band propagation [38,39]. Due to the alternating stress field in the matrix caused by the crystalline precipitates, the otherwise planar shear band is forced to change its direction in an oscillating manner [31,38,39] and therefore the effective free path between neighbouring particles becomes even smaller, as sketched in Fig. 8. The interaction between shear bands and nanocrystals might prevent the formation of a single runaway shear band and in addition crack generation can be retarded [28,40]. A nascent shear band must detour around the crystalline obstacles and hence tends to branch or to be blocked [31]. This could be responsible for the lack of extensive shear banding in the present case (Fig. 2) and instead cause the B2 nanocrystals to constantly precipitate during deformation.

To sum up, the growth of the B2 CuZr nanocrystals, the strong interface between crystals and glass, the proper particle size as well as the proper inter-particle spacing are believed to be the origin of the tensile ductility observed in the present experiments.

3.3. Twinning of B2 CuZr nanocrystals

The grain size of the B2 CuZr nanocrystals is not only crucial for the effective suppression of shear bands but it also has a strong impact on the stress at which the martensitic transformation/twinning can take place.

Nanometre-scale grains of Al [41] and of Cu [42] are known to deform via twinning and additionally, the martensitic transformation has been found to proceed via twinning in nanometre-size NiTi grains [43]. Even simulations corroborate that twinning is the dominant deformation mechanism in nanoscale systems [31,44]. However, if the grain size is too small, it is expected that even twinning becomes rather difficult. In the alloys investigated, twin-

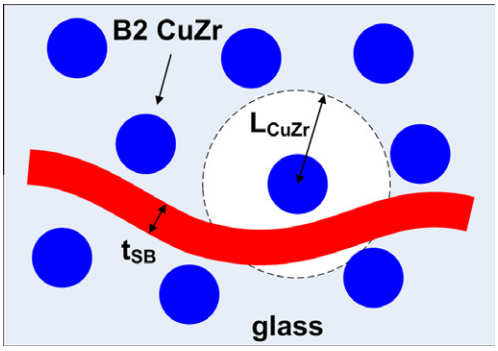

Fig. 8. Schematic showing how the B2 CuZr nanocrystals force the shear band to detour during propagation. The matching of the different length-scales, i.e. shear band thickness, t_{SB}, particle size and inter-particle spacing, L_{CuZr}, ensures that the interaction between shear band and crystals becomes effective.

ning is experimentally observed only for those grains whose diameters, D_{CuZr}, exceed about 20 ± 5 nm (Fig. 4).

The heterogeneous nature of shear banding leads to a stress gradient within the crystalline inclusion and this gradient is calculated to be the larger, the bigger the nanocrystals are [38]. Consequently the stress build-up within the bigger nanocrystals is expected to be higher, and therefore, only the shear modulus in the larger grains softens sufficiently for twinning to occur [30].

Recent results [43] show that twinning in nanocrystals embedded in a glassy matrix is not a collective transformation but instead starts at the crystalline/glassy interface, due to the matrix constraint. The same can be assumed to hold for the present case of B2 CuZr nanocrystals embedded in a glassy matrix. Analogously, twinning starts from an interface in nanocrystalline metals [41,45], where partial dislocations are emitted from the grain boundaries and induce the formation of twins within the grain. Chen et al. [41] have proposed an expression to derive the critical stress for this emission of partial dislocations in nanocrystalline metals. Because twinning in nanoscale particles is somewhat similar to twinning in nanoscale grains, Chen et al.s expression [41] can be adopted here in order to calculate the critical grain size, D^c_{CuZr}, below which twinning is most unlikely to occur:

$$N\tau_p = \frac{2\alpha G b_p}{D_{CuZr}} + \frac{\gamma_{sf}}{b_p} \tag{4}$$

where τ_p is the shear stress needed to nucleate partial dislocations in the CuZr nanocrystals of size D_{CuZr}, N is an effective stress concentration, which is used to consider the promotion effect of the local stress concentration on the twinning formation, α is a parameter reflecting the character of the dislocation (0.5–1.5), G is the shear modulus of B2 CuZr (32 GPa [13,46]), b_p is the magnitude of the Burgers vectors of the partial dislocations ($\sim 9.5 \times 10^{-2}$ nm [47,48]) and γ_{sf} is the stacking fault energy.

The local stress, τ_p, can be related to the macroscopically applied stress, σ_p, as $M\tau_p = \sigma_p$, where M is the Taylor factor. Eq. (4) can be thus rewritten as:

$$\sigma_p \frac{N}{M} = \frac{2\alpha G b_p}{D_{CuZr}} + \frac{\gamma_{sf}}{b_p} \tag{5}$$

This equation establishes a relationship between the grain size, D_{CuZr}, and the stress necessary to induce a martensitic transformation, respectively a twinning process. A crucial factor in Eq. (5) is the stacking fault energy, γ_{sf}. Fig. 9 contains plots of Eq. (5) with three different values for γ_{sf}, 20 mJ m^{-2}, 40 mJ m^{-2} and 60 mJ m^{-2} [49]. The smaller the particles, the higher the stress necessary to induce twinning. The range of ultimate tensile stresses (Table 1) is also indicated in the plot and assuming a stacking fault energy of 40 mJ m^{-2} the critical grain size, D^c_{CuZr}, is calculated to be about 10 nm, which is lower than value determined experimentally of around 20 ± 5 nm (Fig. 4, Table 1). This difference may be attributable to a lack of collectivity in the twinning process. Eq. (5) has been proposed for a nanograined material, in which the processes taking place in a given grain affect its surrounding grains. In the present case, however, the nanocrystals are isolated and the glassy matrix has a constraining effect, which aggravates twinning. The higher transition barrier results in a larger critical grain size for twinning than Eq. (5) theoretically predicts. This is similar to observations by Waitz and Karnthaler, who found that isolated NiTi nanocrystals embedded in an amorphous matrix have a critical diameter for martensitic transformation larger than that observed for grains of nanocrystalline NiTi [43].

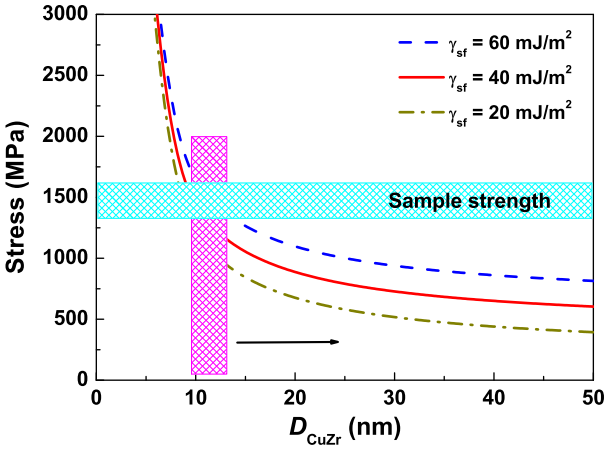

Fig. 9. Stress required to induce twinning in nanocrystalline B2 CuZr as a function of grain size, D_{CuZr}. If the stacking fault energy is assumed to be $\gamma_{sf} = 40$ mJ m^{-2} it follows that at the fracture strength twinning should be induced only in grains larger than about 10 nm. This is lower than the value determined experimentally of $D^c_{CuZr} = 18 \pm 5$ nm and might be due to a lack of collectivity of the twinning process.

The twinning process is capable of further relaxing the stresses in the strained matrix, and thus, it retards the generation of shear bands.

Using the aspects discussed above, one can construct a kind of deformation map for the present Cu–Zr–Al alloys,

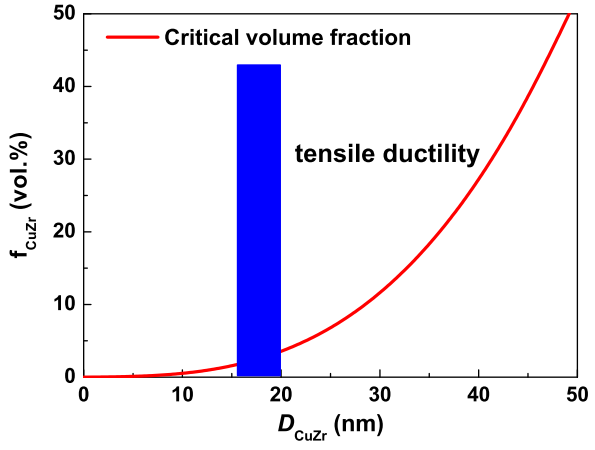

Fig. 10. "Deformation map" of the investigated alloys, indicating the factors that enhance tensile plasticity. The curve represents the critical inter-particle spacing of $L^c_{CuZr} = 60 \pm 10$ nm, which is a function of the particle diameter, D_{CuZr}, and the crystalline volume fraction. The bar indicates the experimentally determined critical grain size, $D^c_{CuZr} = 20 \pm 5$ nm, required for twinning to take place.

as depicted in Fig. 10. It establishes the microstructural region curtailed by the bar and the curve, for which tensile plasticity is expected to occur. The bar represents the experimentally observed critical grain size for twinning $\left(D^c_{\mathrm{CuZr}} = 20 \pm 5\ \mathrm{nm}\right)$ and the curve reflects the critical inter-particle spacing of $L^c_{\mathrm{CuZr}} = 60 \pm 10\ \mathrm{nm}$, which depends on the crystalline volume fraction and the particle size and can be obtained using Eq. (3).

4. Conclusions

The $(Cu_{0.5}Zr_{0.5})_{100-x}Al_x$ ($x = 5$, 6, 8) bulk metallic glasses investigated in this work show a unique tensile deformation behaviour. During loading, metastable B2 CuZr nanocrystals precipitate polymorphically in the matrix and consecutively the crystals larger than about 20 nm undergo twinning. These processes are not restricted to the shear bands but appear to be a bulk phenomenon, which is why the BMGs exhibit a macroscopically detectable ductility accompanied by work-hardening. The shear-induced precipitation of nanocrystals is more pronounced for the BMGs with a lower glass-forming ability and thermal stability. The formation and growth of the nanocrystals and their subsequent twinning hamper the generation and propagation of shear bands on one hand and relax the stress concentrations in the matrix on the other hand. This retards the formation of detrimental shear bands and leads to tensile plasticity.

In principle these processes, which lead to an intrinsic ductility, should be applicable to any bulk metallic glass, which polymorphically precipitates a ductile shape memory compound such as B2 CuZr. The shape memory effect herein guarantees the deformation-induced twinning of the crystals. Most likely this approach can be even extended to BMG matrix composites, which contain face-centred cubic (fcc) or hexagonal close packed (hcp) crystals with the appropriate size for deformation twinning to take place, such as Ti [50], Cu [42] or Al [41] nanocrystals. If these requirements are not met as in the case of Zr-based BMGs [51,52], which are reinforced by a brittle quasi-crystalline phase the mechanical properties cannot be enhanced.

The idea of employing a deformation-induced phase transformation has been successfully applied in the case of another group of intrinsically brittle materials, namely ceramics. Mg partially stabilized zirconia, Mg–PSZ, exhibits a phase transformation from tetragonal to monoclinic, which effectively enhances the toughness of the ceramic [53].

Altogether, the present analysis may be helpful to design advanced bulk metallic glasses that exhibit tensile plastic deformation and work-hardening through a self-toughening mechanism.

Acknowledgements

The authors thank B. Bartusch, U. Wilke, S. Donath, M. Frey, and H. Schulze for technical assistance, and J. Das, H. Ehrenberg, D.C. Hofmann, H.P. Karnthaler, N. Mattern, S. Scudino, M. Stoica, T. Waitz, and M. Zehetbauer for stimulating discussions. Financial support provided by the Global Research Laboratory Program of the Korean Ministry of Education, Science and Technology is gratefully acknowledged. S.P. furthermore acknowledges financial support granted by the program "Promotionsförderung des Cusanuswerks".

References

[1] Schuh CA, Hufnagel TC, Ramamurty U. Acta Mater 2007;55:4067.
[2] Spaepen F. Acta Metall 1977;25:407.
[3] Inoue A. Acta Mater 2000;48:279.
[4] Donovan PE, Stobbs WM. Acta Metall 1981;29:1419.
[5] Zhang Y, Greer AL. Appl Phys Lett 2006;89:071907.
[6] Georgarakis K, Aljerf M, Li Y, LeMoulec A, Charlot F, Yavari AR, et al. Appl Phys Lett 2008;93:031907.
[7] Lewandowski JJ, Greer AL. Nature Mater 2006;5:15.
[8] Masumoto T, Maddin R. Acta Metall 1971;19:725.
[9] Pampillo CA. J Mater Sci 1975;10:1194.
[10] Eckert J, Das J, Pauly S, Duhamel C. J Mater Res 2007;22:285.
[11] Eckert J, Das J, Pauly S, Duhamel C. Adv Eng Mater 2007;9:443.
[12] Pauly S, Das J, Bednarcik J, Mattern N, Kim KB, Kim DH, et al. Scripta Mater 2009;60:431.
[13] Pauly S, Liu G, Wang G, Kühn U, Mattern N, Eckert J. Acta Mater 2009;57:5445.
[14] Pauly S, Liu G, Wang G, Das J, Kim KB, Kuhn U, et al. Appl Phys Lett 2009;95:101906.
[15] Das J, Kim KB, Xu W, Wei BC, Zhang ZF, Wang WH, et al. Mater Trans 2006;47:2606.
[16] Koval YN, Firstov GS, Kotko AV. Scripta Metall Mater 1992;27:1611.
[17] Zhalko-Titarenko AV, Yevlashina ML, Antonov VN, Yavorskii BY, Koval YN, Firstov GS. Phys Status Solidi B 1994;184:121.
[18] Das J, Tang MB, Kim KB, Theissmann R, Baier F, Wang WH, et al. Phys Rev Lett 2005;94:205501.
[19] Wang WH. J Appl Phys 2006;99:093506.
[20] Yang B, Liu CT, Nieh TG. Appl Phys Lett 2006;88:221911.
[21] Yu P, Bai HY. Mater Sci Eng A 2008;485:1.
[22] Kumar G, Ohkubo T, Mukai T, Hono K. Scripta Mater 2007;57:173.
[23] Yu P, Bai HY, Tang MB, Wang WL. J Non-Cryst Solids 2005;351:1328.
[24] Greer AL. Science 1995;267:1947.
[25] Jiang WH, Atzmon M. Acta Mater 2003;51:4095.
[26] Kim JJ, Choi Y, Suresh S, Argon AS. Science 2002;295:654.
[27] Chen H, He Y, Shiflet GJ, Poon SJ. Nature 1994;367:541.
[28] Chen M, Inoue A, Zhang W, Sakurai T. Phys Rev Lett 2006;96:245502.
[29] Zeng KJ, Hämäläinen M, Lukas HL. J Phase Equilib 1994;15:577.
[30] Pauly S, Gorantla S, Wang G, Kühn U, Eckert J. Nature Mater 2010;9:473.
[31] Shi YF, Falk ML. Acta Mater 2008;56:995.
[32] Edington JD. Practical electron microscopy in materials science. London: Van Nostrand Reinhold Company; 1976.
[33] Liu G, Zhang GJ, Ding XD, Sun J, Chen KH. Metall Mater Trans A 2004;35:1725.
[34] Liu G, Zhang GJ, Ding XD, Sun J, Chen KH. Mater Sci Eng A 2003;344:113.
[35] Gurland J. Quantitative microscopy. New York: McGraw-Hill; 1968.
[36] Gilmore DL, Starke EA. Metall Mater Trans A 1997;28:1399.
[37] Cheung TL, Shek CH. J Alloys Compd 2007;434:71.
[38] Lund AC, Schuh CA. Philos Mag Lett 2007;87:603.
[39] Kim KB, Das J, Lee MH, Yi S, Fleury E, Zhang ZF, et al. J Mater Res 2008;23:6.
[40] Lee SW, Huh MY, Fleury E, Lee JC. Acta Mater 2006;54:349.

[41] Chen MW, Ma E, Hemker KJ, Sheng HW, Wang YM, Cheng XM. Science 2003;300:1275.
[42] Lu L, Chen X, Huang X, Lu K. Science 2009;323:607.
[43] Waitz T, Karnthaler HP. Acta Mater 2004;52:5461.
[44] Cheng Q, Wu HA, Wang Y, Wang XX. Appl Phys Lett 2009;95:021911.
[45] Dehm G. Prog Mater Sci 2009;54:664.
[46] Fan GJ, Freels M, Choo H, Liaw PK, Li JJZ, Rhim WK, et al. Appl Phys Lett 2006;89:241917.
[47] Christian JW, Mahajan S. Prog Mater Sci 1995;39:1.
[48] Seo JW, Schryvers D. Acta Mater 1998;46:1165.
[49] Heino P, Perondi L, Kaski K, Ristolainen E. Phys Rev B 1999;60:14625.
[50] Yu Q, Shan ZW, Li J, Huang XX, Xiao L, Sun J, et al. Nature 2010;463:335.
[51] Xing LQ, Eckert J, Löser W, Schultz L. Appl Phys Lett 1999;74:664.
[52] Xing LQ, Bertrand C, Dallas JP, Cornet M. Mater Sci Eng A 1998;241:216.
[53] Porter DL, Heuer AH. J Am Ceram Soc 1977;60:183.